

Models of μ Her with asteroseismic constraints

Wuming Yang¹, Xiangcun Meng¹

^a*School of Physics and Chemistry, Henan Polytechnic University, Jiaozuo 454000, Henan, China.*

Abstract

Using the Yale stellar evolution code, models of μ Her based on asteroseismic measurements are constructed. A χ^2 minimization is performed to approach the best modeling parameters which reproduce the observations within their errors. By combining all non-asteroseismic constraints with asteroseismic measurements, we find that the observational constraints favour a model with a mass of $1.00_{-0.02}^{+0.01} M_{\odot}$, an age $t = 6.433 \pm 0.04$ Gyr, a mixing-length parameter $\alpha = 1.75 \pm 0.25$, an initial hydrogen abundance $X_i = 0.605_{-0.005}^{+0.01}$ and metal abundance $Z_i = 0.0275_{-0.001}^{+0.002}$. μ Her is in post-main sequence phase of evolution. The modes of $l = 1$ show up the characteristics of avoided crossings, which may be applied to test the internal structure of this type stars. Asteroseismic measurements can be used as a complementary constraint on the modeling parameters. **The models with mass 1.00 - 1.10 M_{\odot} can reproduce the observational constraints. Existing observed data of μ Her do not rule out these models.**

Key words: Stars: individual: μ Her, stars: evolution, stars: oscillations

1. Introduction

Solar-like oscillations have been confirmed for several main-sequence and subgiant stars, such as α Cen A (Bedding, 2004), α Cen B (Kjeldsen et al., 2005), Procyon A (Eggenberger et al., 2004b), η Bootis (Carrier et al., 2005), etc. The large and small frequency separations of p-modes can provide a good estimate of the mean density and age of the stars (Ulrich, 1986, 1988). It has been proven that asteroseismology is a powerful tool for determining the fundamental parameters of the stars (Eggenberger et al., 2005; Eggenberger & Carrier, 2006).

μ Her (HR 6623, HD 161797, HIP 86974) is a G5 IV subgiant star, in the neighbourhood of the Sun. It is considered to be a solar-type star with mass $1.14 M_{\odot}$, effective temperature $T_e = 5596 \pm 80$ K, and radius $R = 1.77 \pm 0.07 R_{\odot}$ (Fuhrmann, 1998). Recently, Bonanno et al. (2008) detected solar-like oscillations on μ Her and identified individual frequencies in the range of 900 -

Email address: wuming.yang@hotmail.com (Wuming Yang)

1600 μHz . These seismological data will provide a constraint on the fundamental parameters of μ Her. In this work, we try to determine modeling parameters of μ Her based on asteroseismic constraints using the Yale Rotation Evolution Code (YREC7) in its non-rotating configuration.

The observational constraints available for μ Her are summarized in Sect. 2, while the details of the evolutionary models and the computational method are given in Sect. 3. The results are presented in Sect. 4 and the conclusion is given in Sect. 5.

2. Observational constraints

2.1. Effective temperature, luminosity and chemical composition

The effective temperature of μ Her given by Fuhrmann (1998) is 5596 K, however that given by Ivanov et al. (2004) is only 5390 K. Combining other data (Valdes et al., 2004; Takeda et al., 2005; Soubiran et al., 2008), we adopt an average effective temperature $T_{eff} = 5500 \pm 90$ K.

The luminosity of a star can be obtained through combining the knowledge of the magnitude and distance. By combining the visual magnitude $V = 3.417 \pm 0.014$, the bolometric correction $BC = -0.15 \pm 0.05$ mag (Fuhrmann, 1998), the solar absolute magnitude $M_{bol,\odot} = 4.746$ (Lejeune et al., 1998) and the newest Hipparcos parallax $\Pi = 120.33 \pm 0.16$ mas (Van Leeuwen, 2007), we obtained a luminosity for μ Her of $L = 2.70 \pm 0.16 L_{\odot}$.

In the version of the Catalogue of [Fe/H] determinations given by Cayrel et al (2001), there are five metallicity values for μ Her. Recent determinations give the values: 0.26 (Soubiran & Girard, 2005) and 0.29 (Takeda et al., 2005). We adopt the average of these determinations, $[\text{Fe}/\text{H}] = 0.21 \pm 0.07$. This value is close to the value of 0.23 given by (Fuhrmann, 1998). For Population I stars, the ratio of surface heavy elements to hydrogen abundance is related to the Fe/H by $[\text{Fe}/\text{H}] \simeq \log(Z/X)_s - \log(Z/X)_{\odot}$, where $(Z/X)_{\odot}$ is the ratio of the solar mixture. The most recent ratio of the heavy-element abundance to hydrogen abundance of the Sun, $(Z/X)_{\odot}$, is 0.0171 (Asplund et al., 2004). There are, however, some discrepancies between this new value and seismical results (Yang & Bi, 2007). Thus in this work, we adopt the old value, 0.0245 (Grevesse & Noels, 1993). Consequently, the value of $(Z/X)_s$ for μ Her is about 0.040 ± 0.006 .

2.2. Asteroseismic data

solar-like oscillations for this star have been detected by Bonanno et al. (2008) with the SARG echelle spectrograph. Twenty oscillation frequencies have been identified by using modified and standard extraction methods between 900 and 1600 μHz . By means of a least square best fit with the asymptotic relation of frequencies for all the identified modes, Bonanno et al. (2008) gave that the most likely value of the mean large and small frequency separation is $\Delta\nu = 56.50 \pm 0.07$ μHz and $\delta\nu = 5.03 \pm 0.94$ μHz , respectively. Some of the observational constraints for μ Her used in this work are given in Table 1.

Table 1: Observational data for μ Her used in this work.

Π [mas]	120.33 ± 0.16
V [mag]	3.417 ± 0.014
L/L_{\odot}	2.70 ± 0.16
T_{eff} [K]	5500 ± 90
$[Fe/H]_s$	0.21 ± 0.07
$\Delta\nu$ [μ Hz]	56.50 ± 0.07
$\delta\nu$ [μ Hz]	5.03 ± 0.94

3. Stellar models

3.1. Input physics

A grid of stellar evolutionary models was computed with the YREC7 in its non-rotating configuration (Guenther et al., 1992). All models are evolved from fully convective pre-main sequence (PMS) to a stage of subgiant. The OPAL EOS2001 (Rogers & Nayfonov, 2002), OPAL opacity (Iglesias & Rogers, 1996), and the Alexander & Ferguson (1994) opacity for low temperature were used. These opacity tables have the solar mixtures given by Grevesse & Noels (1993). The models took into account diffusion of helium and metals, using the prescription of Thoul et al. (1994). Energy transfer by convection is treated according to the standard mixing-length theory, and the boundaries of the convection zones are determined by the Schwarzschild criterion. See Demarque et al. (2007) in details for the YREC.

3.2. Computational method

The position of a stellar model in the Hertzsprung-Russell (H-R) diagram depends on five modeling parameters: the stellar mass M , the mixing-length parameter α , the age of the star t , the initial hydrogen abundance X_i and metallicity Z_i . For μ Her we take the ratio of the heavy-element abundance to hydrogen abundance on the stellar surface as an observable. Thus we have three observables ($L, T_{eff}, (Z/X)_s$) and five unknowns (M, α, t, X_i, Z_i).

In order to reproduce the observational constraints, we construct a grid of models with various masses, initial element abundances and mixing-length parameters. For each stellar model, low-degree p-mode frequencies are computed using Guenther adiabatic pulsation code (Guenther, 1994). To find the set of modeling parameters (M, α, Z_i, X_i, t) that leads to the best agreement with the observational constraints, following Eggenberger et al. (2004a), we perform a χ^2 minimization. The function χ^2 is defined as follows

$$\chi^2 = \chi_{clas}^2 + \chi_{osci}^2, \quad (1)$$

where

$$\chi_{clas}^2 = \left(\frac{T_{mod}^{eff} - T_{obs}^{eff}}{\sigma(T_{obs}^{eff})} \right)^2 + \left(\frac{\log(\frac{L}{L_{\odot}})_{mod} - \log(\frac{L}{L_{\odot}})_{obs}}{\sigma(\log(\frac{L}{L_{\odot}})_{obs})} \right)^2 + \left(\frac{[\frac{Fe}{H}]_{mod} - [\frac{Fe}{H}]_{obs}}{\sigma([\frac{Fe}{H}]_{obs})} \right)^2, \quad (2)$$

and

$$\chi_{osci}^2 = \frac{1}{N} \sum_{i=1}^N \left(\frac{\nu_i^{theo} - \nu_i^{obs} - \langle D_{\nu} \rangle}{\sigma} \right)^2. \quad (3)$$

Here the $\sigma()$'s are the errors on the corresponding observations, N is the number of observed frequencies, $\sigma = 1.8 \mu\text{Hz}$ is the resolution on the observed frequencies, and $\langle D_{\nu} \rangle = \sum_{i=1}^N (\nu_i^{theo} - \nu_i^{obs})/N$. The model which can minimize χ_{clas}^2 and χ_{osci}^2 at the same time will be considered to be the best one.

4. Results

Firstly, we computed a grid of evolutionary tracks for models with masses, mixing length parameters, initial metal and hydrogen mass fractions respectively in the ranges of $0.86 M_{\odot} \leq M \leq 1.16 M_{\odot}$, $1.5 \leq \alpha \leq 2.10$, $0.025 \leq Z_i \leq 0.033$, $0.57 \leq X_i \leq 0.70$ **with a primary resolution** $\delta M = 0.02$, $\delta \alpha = 0.2$, $\delta Z = 0.002$, **and** $\delta X = 0.02$. Computational results show that the evolutionary tracks for models with $0.9 M_{\odot} < M < 1.15 M_{\odot}$ and $1.5 \leq \alpha \leq 2.10$ approximately span the error box in $[T_{eff}, L, (Z/X)_s]$. This is because the fact that a decrease of the mass can be compensated by a decrease in hydrogen and metal abundances to get the same position in the H-R diagram (Meng et al., 2008). Moreover, the evolutionary tracks imply that μ Her is in the post-main sequence phase of evolution. In this phase, the tracks are almost parallel to the T_{eff} -axis (see Figs. 1, 2). Additionally, a variation of the mixing length parameter mainly changes the radius, but has almost no influence on the luminosity (Kippenhahn & Weigert, 1990). Therefore, with increasing the mixing length parameter α , the evolutionary track moves almost horizontally to the left of H-R diagram and vice versa. Thus the models with various mixing length parameters can span the same position in the H-R diagram (see Fig. 2) at different ages. Table 3 gives the characteristics of three models, M2a, M2 and M2b, with different mixing length parameters but a same surface metallicity and position in the H-R diagram. These models have different χ_{osci}^2 , i.e. different oscillation frequencies, reflecting the differences in the internal structure of the models; for example, the differences in the central helium-core mass and density. This indicates that non-asteroseismic observational constraints do not enable us to determine the mixing-length parameter α for μ Her, an evolved solar-type star, but asteroseismic observations could provide a constraint on the mixing length parameter.

For the sets of modeling parameters that lead to agreements with the observational constraints, we calculated the models with a fine resolution $\delta M = 0.01$, $\delta \alpha = 0.05$, $\delta Z = 0.0005$, **and** $\delta X = 0.005$ **in the vicinity of the parameters. We obtained many models that can almost**

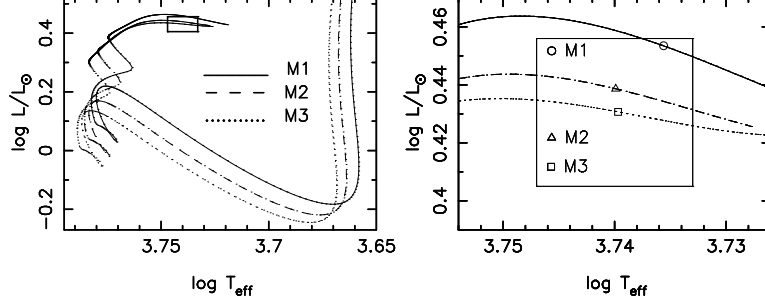


Figure 1: Evolutionary tracks in the H-R diagram for models of μ Her. Left panel: full tracks. Right panel: close-up of H-R diagram in the vicinity of μ Her. The positions in the H-R diagram of the models listed in Table 2 are indicated. The box shows the position of μ Her.

Table 2: Models for μ Her. The superscripts or subscripts of some modeling parameters show confidence limits.

Observational constraints	$\log L/L_{\odot}$	0.431 ± 0.025		
	T_{eff} [K]	5500 ± 90		
	$(Z/X)_s$	0.040 ± 0.006		
	$\Delta\nu$	56.50 ± 0.07		
Modeling parameters	M/M_{\odot}	M1	M2	M3
	α	$1.10_{-0.01}$	$1.00^{+0.01}_{-0.02}$	0.93 ± 0.015
	Z_i	1.75 ± 0.25	1.75 ± 0.25	1.75 ± 0.25
	X_i	$0.029^{+0.001}$	$0.0275^{+0.002}_{-0.001}$	0.026 ± 0.002
Model characteristics	$\log L/L_{\odot}$	0.4550	0.4386	0.4307
	T_{eff} [K]	5454	5494	5492
	Z_s	0.0272	0.0257	0.0245
	$(Z/X)_s$	0.040	0.040	0.041
	R/R_{\odot}	1.894	1.831	1.816
	age [Gyr]	6.556 ± 0.03	6.433 ± 0.04	6.303 ± 0.03
	χ^2_{osci}	1.05	1.07	4.55
	χ^2_{clas}	1.18	0.10	0.03
	χ^2	2.23	1.17	4.58
	$\Delta\nu_0$	56.44	56.58	55.34
	$\delta\nu_{02}$	5.00	4.94	5.09
	$\langle D_{\nu} \rangle$ [μ Hz]	28.10	31.20	-0.53
	He-core mass [M_{\odot}]	0.100	0.101	0.105

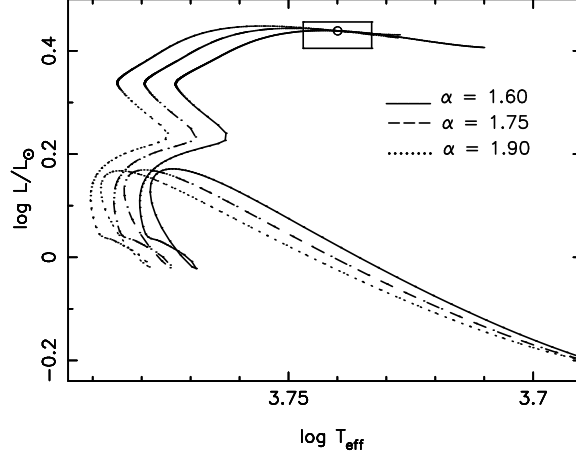


Figure 2: Evolutionary tracks in the H-R diagram for models with $Z_i = 0.0275$, $X_i = 0.605$, and $M = 1.00 M_\odot$, with the lines differing in the value of the mixing-length parameter, α . The box shows the position of μ Her. Open circles indicate the locations of the M2a, M2 and M2b models listed in Table 3.

Table 3: Characteristics of the models illustrated by open circles in Fig.2.

	M2a	M2	M2b
M/M_\odot	1.00	1.00	1.00
Z_i	0.0275	0.0275	0.0275
X_i	0.605	0.605	0.605
α	1.60	1.75	1.90
age [Gyr]	6.374 ± 0.04	6.433 ± 0.04	6.471 ± 0.03
$\log L/L_\odot$	0.4387	0.4386	0.4387
T_{eff} [K]	5494	5494	5493
$(Z/X)_s$	0.040	0.040	0.041
R/R_\odot	1.832	1.831	1.832
χ_{clas}^2	0.099	0.097	0.101
χ_{osci}^2	3.50	1.07	3.37
$\Delta\nu_0$	56.65	56.58	56.46
$\log \rho_c$ [g/cm^3]	3.636	3.800	3.942
He-core mass [M_\odot]	0.091	0.101	0.109

minimize the χ_{osci}^2 and fall within the observational error box. Fig. 3 shows the χ_{osci}^2 as a function of mass and age. From this figure we can see that the models with mass 1 - 1.1 M_{\odot} and age 6.2 - 6.7 Gyr can better reproduce the observed frequencies. We also constructed the models with higher resolutions of modeling parameters than the fine resolution. But results are not sensitive to the resolutions. Performing the χ^2 minimization described above, we found a solution: $M = 1.00 M_{\odot}$, $\alpha = 1.75$, $Z_i = 0.0275$, $X_i = 0.605$, and $t = 6.433$ Gyr, marked M2. Table 2 lists characteristics of this model. **The confidence limits of each modeling parameter correspond to the maximum/minimum values it can reach when other parameters are fixed, in order that the generated models fall within the observational error box.** Corresponding evolutionary tracks are shown in Figure 1. Although the value of χ_{clas}^2 and χ_{osci}^2 of the M2 model is not the lowest one respectively, this model is almost able to minimize χ_{clas}^2 and χ_{osci}^2 at the same time and has a lowest χ^2 . **Fig. 3 shows the model with a mass of 1.04 M_{\odot} has a lowest χ_{osci}^2 . But the value of χ^2 of this model is larger than that of M2.** The mean large and small separation of the M2 model is 56.58 and 4.94 μHz , respectively, which are in good agreement with those observed. However, the mass of M2 model, 1.00 M_{\odot} , is less than the values given by Fuhrmann (1998) and Takeda et al. (2005). They showed that the mass of μ Her is about 1.14 M_{\odot} . Table 2 also gives a model M1 which has a mass as high as 1.10 M_{\odot} . This model is able to minimize χ_{osci}^2 in the age of 6.556 Gyr but has a higher value of χ_{clas}^2 . This implies that increasing the hydrogen abundance and mass at the same time for a fixed value of the mixing length parameter leads to an increase in the χ_{clas}^2 in order to attain the same value of χ_{osci}^2 . This scenario was also found by Eggenberger & Carrier (2006). The mean large and small separation of the M1 model is 56.44 and 5.00 μHz , respectively, which are almost same as those of the M2 model.

In Fig. 4, we plotted the differences between the observed and theoretical frequencies for the M1 and M2 model. Moreover, the theoretical and observed frequencies are compared by plotting echelle diagrams of the M1 and M2 models in Fig. 5. The systematic difference $\langle D_{\nu} \rangle$ between computed and observed frequencies has been considered in these figures. The systematic difference $\langle D_{\nu} \rangle$ is 28.1 and 31.2 μHz for the M1 and M2 models, respectively. This systematic difference also exists in other stellar models (Christensen-Dalsgaard et al., 1995; Eggenberger et al., 2004a,b; Eggenberger & Carrier, 2006). Fig. 4 shows that the differences between the observed and theoretical frequencies are very similar for both models at high frequency, however they are different at lower frequency. Compared to the M2 model, the M1 model badly reproduces the observed frequencies of 1034.0 and 1061.2 μHz , whereas the M2 model does not reproduce the observed frequencies of 947.6 and 1124.8 μHz well. These comparisons between individual observed and theoretical asteroseismic frequencies for the M1 and M2 models do not allow us to differentiate which model is better. Additionally, both models have the almost same values of the mean large and small separations reflecting a similarity of the internal structure between the M1 and M2 models. For example, both models have an almost same helium-core

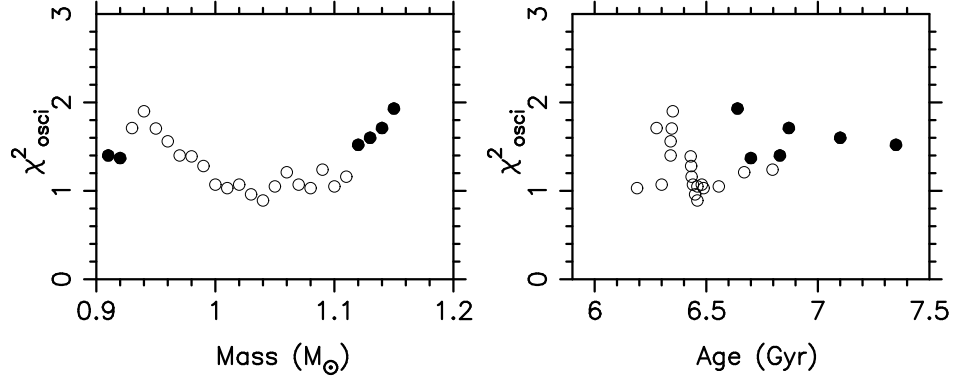


Figure 3: Lowest values of χ_{osci}^2 as a function of mass and age. Open circles indicate models in accordance with the classical observational constraints, while dots show models that do not fall within the observational error box.

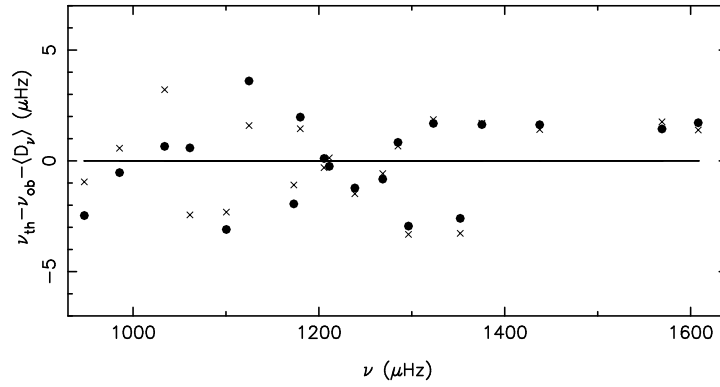


Figure 4: Differences between computed and observed frequencies. Crosses and filled circles correspond to the M1 and M2 model, respectively. The systematic difference $\langle D_\nu \rangle$ has been taken into account in this figure.

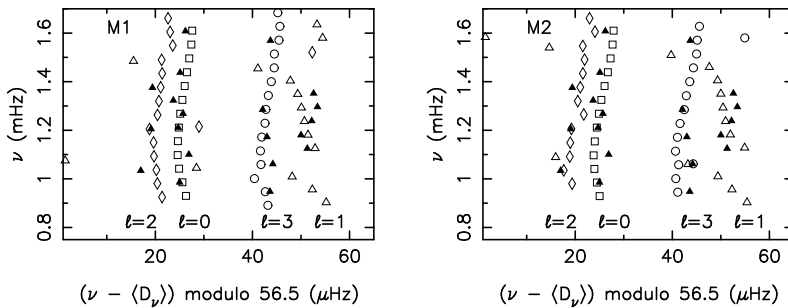


Figure 5: Echelle diagrams for the M1 and M2 model, respectively. Filled triangles refer to the observed frequencies (Bonanno et al., 2008), while open symbols correspond to the theoretical ones. Squares are used for modes with $l = 0$, triangles for $l = 1$, diamonds for $l = 2$ and circles for $l = 3$.

mass.

However, Fig. 5 shows that both the M1 and M2 models badly reproduce the observed frequencies of $l = 1$. We searched the models which can better reproduce the observed frequencies of $l = 1$. A model labeled M2b, which was shown in Table 3, was found. However, the value of χ_{osci}^2 for the M2b model is larger than **those** of the M1 and M2 models, which is mainly due to differences in the modes of $l = 1$ of these models. If the contribution to χ_{osci}^2 from the $l = 1$ mode near $1238 \mu\text{Hz}$ is neglected, the value of χ_{osci}^2 for the M2b model will decrease from 3.37 to 0.72. Echelle diagram for the M2b model is shown in Fig. 6. Except for the $l = 1$ mode near $1238 \mu\text{Hz}$, the M2b model reproduces the observed frequencies well. Moreover Fig. 6 shows that the observed and theoretical frequencies with $l = 1$ have a similar behavior: **a zigzag echelle diagram**. The modes of $l = 1$ show up a deviation from their expected asymptotic values. Fig. 7 also shows that the large separations for modes of $l = 1$ deviate from their expected asymptotic behaviour. This may be because that the formation of the central helium core leads to an increase in the frequencies of the g-modes. ‘When the frequency of a g-mode approaches that of a p-mode, the two modes undergo an avoided crossing, where they exchange physical nature’ (Aizenman et al., 1977; Christensen-Dalsgaard et al., 1995). Figs. 6 and 7 show that the $l = 1$ modes of the M2b model between 1200 and $1300 \mu\text{Hz}$ may undergo the avoided crossing. Noting the helium-core mass of the M1 and M2 models are almost same, but that of the M2 and M2b models are different, the behaviour of the $l = 1$ modes might be very sensitive to the internal structure of the stars. It may be applied to extract the information of the helium core.

We also considered a χ_{osci}^2 which does not contain $\langle D_\nu \rangle$. For models falling within the observed constraints on effective temperature, luminosity and surface metallicity, we computed this new χ_{osci}^2 . A solution with $M = 0.93 M_\odot$, $\alpha = 1.75$, $Z_i = 0.026$, $X_i = 0.572$, and $t = 6.303 \text{ Gyr}$ was found. The evolutionary track and the position of this model (marked M3) in the H-R diagram are also

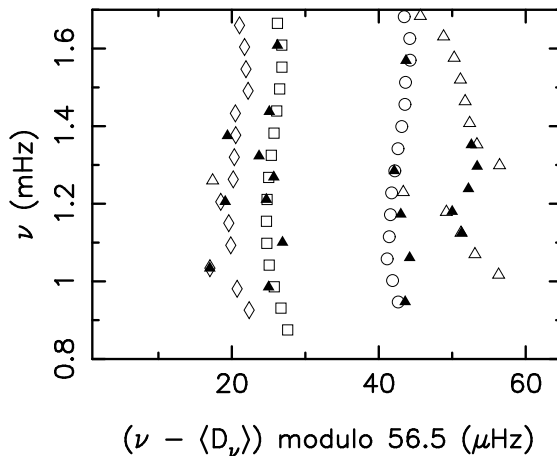


Figure 6: Echelle diagrams for the M2b model. Filled triangles refer to the observed frequencies (Bonanno et al., 2008), while open symbols correspond to the theoretical ones. Squares are used for modes with $l = 0$, triangles for $l = 1$, diamonds for $l = 2$ and circles for $l = 3$. The systematic shift $\langle D_\nu \rangle$ is $28.4 \mu\text{Hz}$ for this model.

shown in Fig. 1. The characteristics of the M3 model are given in Table 2. The systematic difference $\langle D_\nu \rangle$ between computed and observed frequencies is $-0.53 \mu\text{Hz}$ for this model. However the value of the new χ_{osci}^2 is 4.55, which is much larger than that of the M1 and M2 models. Moreover the echelle diagram of the M3 model is plotted in Fig. 8. This echelle diagram shows that the M3 model can reproduce the frequencies in the range of $1034 < \nu < 1437 \mu\text{Hz}$ but badly reproduces the modes at the lower and higher frequencies. Moreover its mean larger separation is only $55.49 \mu\text{Hz}$. Thus this model is in disagreement with the asteroseismic constraints.

5. Discussion and Conclusion

The mass of $1.00 M_\odot$ for the M2 and M2b models is less than the value in the previous literatures (Fuhrmann, 1998; Takeda et al., 2005), which may result from that the results of Fuhrmann (1998) and Takeda et al. (2005) were obtained without the asteroseismic constraints. The initial hydrogen mass fraction is 0.605 and 0.650 for the M2 and M1 model, respectively. Although there is a difference of 0.0015 in Z between the M1 and M2 model, the increase of the hydrogen or decrease of helium is mainly compensated by an increase of the mass in order to reach the same location in the H-R diagram: a helium-mass degeneracy (Lebreton et al., 1993). The M1 and M2 models have the same value of χ_{osci}^2 and the almost same asteroseismic features. This implies that the helium-mass degeneracy is difficult to be removed, even if the asteroseismic constraints are taken into account.

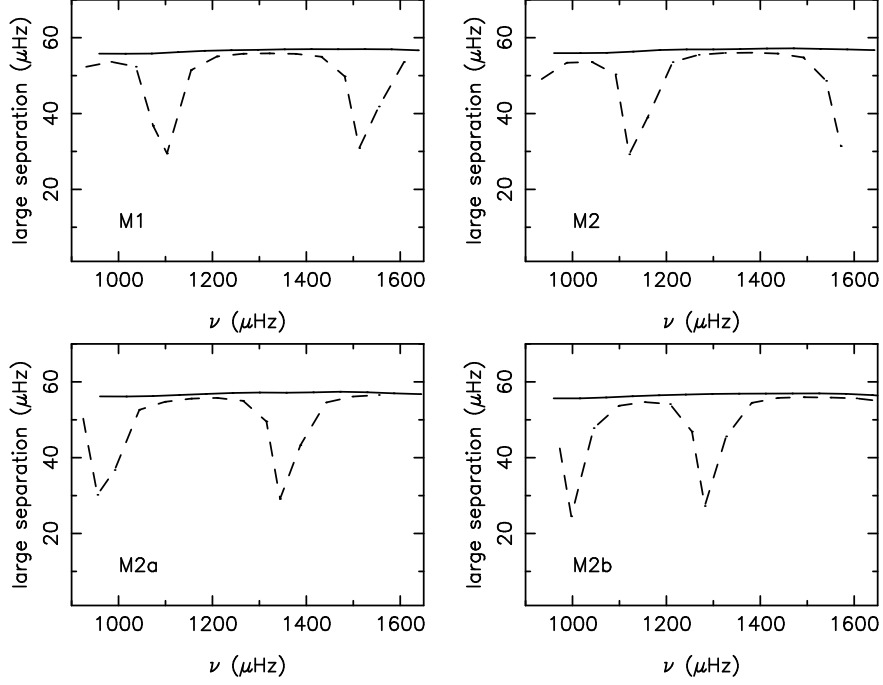


Figure 7: Large separations of theoretical frequencies of different models. The solid line shows the large separations of the $l = 0$ modes, while the dashed line indicates the large separations of the $l = 1$ modes.

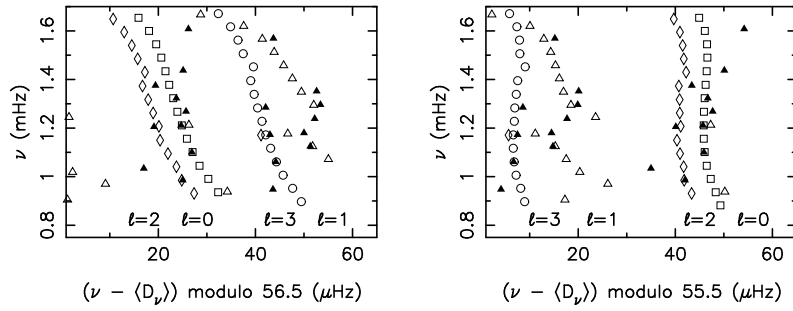


Figure 8: Same as Fig. 5, but for the M3 model. Left panel shows frequencies modulo the value of observed large separation, while right panel presents frequencies modulo the value of theoretical large separation.

Comparing with the observed frequencies, the theoretical frequencies have a systematic shift. **The mode of $l = 1$ near 1238 μHz deviate from its expected asymptotic value in Fig. 6. It may undergo an avoided crossing and be a mixed-mode. The mixed-mode could have higher inertia than other p-modes. The shift of this mode may be different from that of other p-modes. Thus we divide the χ_{osci}^2 into two parts: one χ_{oscm}^2 for mixed-modes and one χ_{oscp}^2 for all modes except for mixed-modes. Assuming only the $l = 1$ mode near 1238 μHz is a mixed-mode, we obtained the value of this new χ_{osci}^2 is 1.07, 1.10, 3.61 and 0.72 for M1, M2, M2a and M2b, respectively. Under this assumption, M2b has a smallest χ_{osci}^2 .**

We confirmed the results that an analysis of the H-R diagram does not allow us to determine the mixing length parameter for an evolved solar-type star (Fernandes & Monteiro, 2003) but the observed oscillation frequencies could provide a constraint on this parameter. The internal structure of the evolved solar-type stars is sensitive to the mixing length parameter at given (T_{eff}, L) .

In this work we constructed the models for the μ Her using the Yale stellar evolution code. By combining the non-asteroseismic constraints with the asteroseismic observations, we find that a model for μ Her can reproduce the all non-asteroseismic and asteroseismic constraints well: **the model with a mass of $1.00_{-0.02}^{+0.01} M_{\odot}$, an age $t = 6.433 \pm 0.04$ Gyr, a mixing-length parameter $\alpha = 1.75 \pm 0.25$, an initial hydrogen abundance $X_i = 0.605_{-0.005}^{+0.01}$ and metal abundance $Z_i = 0.0275_{-0.001}^{+0.002}$. However, the models with mass 1 - 1.1 M_{\odot} and age 6.2 - 6.7 Gyr also can reproduce the non-asteroseismic and asteroseismic constraints. Existing observational constraints do not rule out those models.**

The modes of $l = 1$ show up the characteristic avoided crossings, which may be applied to test the internal structure of an evolved solar-type star. The asteroseismic observations put important constraints on the models for μ Her, but they are not enough to really test the differences in the models. More accurate oscillation frequencies, especially the modes of $l = 1$, are need to investigate the internal structure of this type star.

References

- Alexander, D. R., & Ferguson, J. W. 1994, ApJ, 437, 846
- Asplund, M., Grevesesse N., Sauval, A. J., Allende Prieto, C., & Kiselman, D. 2004, A&A, 417, 751
- Aizenman, M., Smeyers, P., & Weigert. A. 1977, A&A, 58, 41
- Bedding, T. R., Kjeldsen, H., Butler, P. R., et al. 2004, ApJ, 614, 380
- Bonanno, A., Benatti, S., & Claudi, R. et al. 2008, ApJ, 676, 1248
- Carrier, F., Eggenberger, P., & Bouchy, F. 2005, A&A, 434, 1085

- Cayrel, D. S. G., Soubiran, C., & Ralite, N. 2001, *A&A*, 373, 159
- Christensen-Dalsgaard, J., Bedding, T. R., & Kjeldsen, H. 1995, *ApJ*, 443, L29
- Demarque, P., Guenther, D. B., Li, L. H., Mazumdar, A., & Straka, C. W. 2007, *AP&SS*, 316, 31
- Eggenberger, P., Charbonnel, C., & Talon, S. et al. 2004a, *A&A*, 235, 246
- Eggenberger, P., Carrier, F., Bouchy, F. & Blecha, A. 2004b, *A&A*, 422, 247
- Eggenberger, P., Carrier, F., & Bouchy, F. 2005, *NewA*, 10, 195
- Eggenberger, P., & Carrier, F. 2006, *A&A*, 449, 293
- Fernandes, J., & Monteiro, M. J. P. F. G. 2003, *A&A*, 399, 243
- Fuhrmann, K. 1998, *A&A*, 338, 161
- Grevesse, N., & Noels, A. 1993, in *Origin and Evolution of the Elements*, ed. N. Prantzos, E. Vangioni-Flam, & M. Cassé (Cambridge University Press), p15
- Guenther, D. B., Demarque, P., Kim, Y.-C., & Pinsonneault, M. H. 1992, *ApJ*, 387, 372
- Guenther, D. B. 1994, *ApJ*, 422, 400
- Iglesias, C., & Rogers, F. J. 1996, *ApJ*, 464, 943
- Ivanov, V. D., Rieke, M. J., & Engelbracht, C. W. et al. 2004, *ApJS*, 151, 387
- Kippenhahn, R., & Weigert, A. 1990, in *Stellar Structure and Evolution* (Berlin, Springer-Verlag), p271
- Kjeldsen, H., Bedding, T. R., & Butler, R. P. et al. 2005, *ApJ*, 635,1281
- Lebreton, Y., Auvergne, M., & Morel, P. 1993, in *Inside the Stars*, IAU Coll. 137, ed. A. Baglin, & W. W. Weiss, ASP Conf. Ser., 40, 474
- Lejeune, T., Cuisinier, F., & Buser, R. 1998, *A&AS*, 130, 65
- McWilliam, A. 1990, *ApJS*, 74, 1075
- Meng, X., Chen, X., & Han, Z. 2008, *A&A*, 487, 625
- Rogers, F. J., & Nayfonov, A, *ApJ* 2002, 576,1064
- Soubiran, C., & Girard, P. 2005, *A&A*, 438, 139
- Soubiran, C., Bienayme, O., Mishenina, T. V., & Kovtyukh, V. V. 2008, *A&A*, 480, 91
- Takeda, Y., Ohkubo, M., & Sato, B. et al. 2005, *PASJ*, 57, 27

- Thoul, A. A., Bahcall, J. N., Loeb, A. 1994, ApJ, 421, 828
- Ulrich, R. K. 1986, ApJL, 306, L37
- Ulrich, R. K. 1988, IAUS, 123, 2990
- Valdes F., Gupta R., Rose J.A., Singh H.P., Bell D.J. 2004, ApJS,152, 251
- Van Leeuwen, F. 2007, A&A, 474, 653
- Yang, W. M., & Bi, S. L. 2007, ApJ, 658, L67